Identifying the seeding signature in cloud particles from hydrometeor residuals

Mahen Konwar[1*], Benjamin Werden[2,], Edward C. Fortner[2], Sudarsan Bera[1], Mercy Varghese[1], Subharthi Chowdhuri[1,&], Kurt Hibert[3], Philip Croteau[2], John Jayne[2], Manjula Canagaratna[2], Neelam Malap[1], Sandeep Jayakumar[1], Shivsai A. Dixit[1], Palani Murugavel[1], Duncan Axisa[4], Darrel Baumgardner[5], Peter F. DeCarlo[6], Doug R.Worsnop[2], and Thara Prabhakaran[1]

[1] Indian Institute of Tropical Meteorology, Ministry of Earth Sciences, Pune, India 411008

[2]Aerodyne Research Inc., Billerica, MA, USA, 01821

[3]Weather Modification Inc., Fargo, ND, USA, 58102

[4]Center for Western Weather and Water Extremes, Scripps Institution of Oceanography, La Jolla, CA 92037, USA

[5] Droplet Measurement Technologies, Longmont, CO, USA, 80503

[6]Department of Environmental Health and Engineering, Johns Hopkins University, Baltimore, MD USA 21218

[&]now at University of California, Irvine, CA 92697-2700, USA

*Corresponding author

Dr. Mahen Konwar

Indian Institute of Tropical Meteorology

Dr. Homi Bhabha Road, Pune 411 008, India.

Email: mkonwar@tropmet.res.in

Abstract:

Cloud seeding experiments for modifying clouds and precipitation have been underway for nearly a century; yet practically all the attempts to link precipitation enhancement or suppression to the presence of seeding materials within clouds remain elusive. In 2019, the Cloud-Aerosol Interaction and Precipitation Enhancement Experiment (CAIPEEX) investigated residuals of cloud hydrometeors in seeded and non-seeded clouds with an airborne mini-Aerosol Mass Spectrometer (mAMS). The mAMS was utilized in conjunction with a counterflow virtual impactor (CVI) inlet with a cutoff diameter size of approximately 7 μm. The evaporated cloud droplets from the CVI inlet as cloud residuals were evaluated through the mAMS. The Chlorine (Cl) associated with hygroscopic materials, i.e., Calcium Chloride ($CaCl_2$) and potassium (K), which serve as the oxidizing agents in the flares, is found in relatively higher concentrations in the seeded clouds compared to the non-seeded clouds. In convective clouds, Cl and K as cloud residuals were found even at an distance 2.25 km from the cloud base. Major findings from the seeding impact are: an increase in the number concentration of small (<20 μm) droplets and an indication of raindrop formation at 2.25 km above the cloud base. It is demonstrated that the seed particle signature can be traced inside clouds along with the microphysical impacts.

1. Introduction:

E.G. Bowen first proposed in 1952 that hygroscopic particles can foster collision-coalescence (CC) processes in a cloud (Bowen, 1952). Since then, cloud seeding experiments have been conducted worldwide to mitigate and respond to the ever-increasing urban water demand during a drought season or in drought-prone regions. More than 50 countries are involved in weather modification projects (Flossmann, et al., 2019). Over the years, the interest in rain enhancement projects has increased due to the accumulating evidence of a potentially positive effect (i.e., enhancement in rainfall) in several seeding experiments (Mather et al., 1996; Mather et al. 1997; Bruintjes, 1999; WMO, 2000; Gayatri et al., 2023; Prabhakaran et al., 2023). However, skepticism remains within the broader cloud physics community because the efficacy of many cloud seeding experiments remains inconclusive (Ryan and King, 1997; Silverman, 2003; Flossmann et al., 2019). In addition to the existing challenges of evaluating the effectiveness of cloud seeding experiments, other pivotal longstanding issues revolve around accurately detecting the hygroscopic particles released within a cloud, identifying the seeded cloud, and comprehending the impact of seeding on the cloud microphysical properties.

Traditionally, in a cloud seeding experiment tracers such as the inert gas, sulfur hexafluoride (SF_6) (Stith, et al., 1986; Stith et al., 1990; Bruintjes et al., 1995; Rosenfeld et al., 2010), or radar chaff at cloud bases are released, and then efforts are made to measure these tracers higher in the cloud. However, tracing of SF_6 in a seeded cloud is challenging and successful trials have been reported only on a few occasions near the cloud base (Rosenfeld et al., 2010). The detection of SF_6 and chaff traces is hampered by detection limits, especially in the presence of high background concentrations. Using these tracers as proxies for tracking air masses carrying seeding material is limited by the challenge of unambiguously connecting their presence with the seeding material due

to their non-reactive nature with cloud particles. Consequently, several questions arise during these experiments. For instance, does the dispersed seeding material effectively enter the targeted cloud region? Up to what altitude do these materials reach? Are the in-situ measurements being conducted within the intended cloud volume? How can transported flare particles be located within large clouds? Due to these uncertainties the need to more quantitatively evaluate the direct link between seeding materials and the formation of cloud hydrometeors, the development of a low-impact but more effective tracer has been recommended, e.g. Tessendorf et al., (2012).

A critical question in any cloud seeding experiment is whether the observed changes in the cloud microphysical properties after seeding are due to the introduction of seeding material or to natural cloud processes. There are two requirements necessary to address this question: (i) Can the trajectory of seeding material be successfully traced in the cloud, and (ii) can changes in cloud microphysical processing be linked to seeding materials? In this study, an instrumented aircraft was deployed to acquire convincing evidence that addresses these questions. This work primarily addresses how to trace seed particles' signatures in clouds and focuses on the question of changes in cloud micrpphysical properties due to the introduction of seeding particles. This novel technique uses a mini-Aerosol Mass Spectrometer (mAMS) (Jayne et al., 2000) behind a counterflow virtual impactor (CVI) (Noone et al., 1988; Shingler et al., 2012) to identify seeding material in the cloud droplets residuals i.e., the aerosols that remain after evaporation of the cloud droplets.

The hygroscopic cloud seeding hypothesis relies on a chain of microphysical processes. Dispersal of giant cloud condensation nuclei (CCN), hygroscopic particles with diameter between 1-10 μm, in the updraft region of cloud base adds larger drops to the tail of the natural cloud droplet size distribution (DSD), known as the 'tail effect'. This effect further accelerates the formation of raindrops through CC (Segal et al., 2004; Segal, et al., 2007; Kuba and Murakami, 2010; Konwar et

al, 2023). With the initial activation and growth of these larger CCN, the supersaturation over water droplets (SS_w) decreases above the cloud base. As a result, the smaller, natural CCN do not activate. This effect reduces the total droplet number concentration (N_t, cm^{-3}) and broadens the DSDs, a phenomenon known as the 'competition effect' . This broadening fosters the droplet growth rate by intensifying the CC process, which accelerates the formation of precipitation (Cooper et al., 1997; Rosenfeld et al., 2010). Past studies used in-situ measurements to evaluate well-formed seeded clouds whose formation revealed a broadening of the DSDs by hygroscopic seeding in marine stratocumulus clouds (Ghate et al., 2007). Researchers reported that an increased concentration of small cloud droplets occurred at an earlier stage, while at a later stage, an increased concentration in the large size range of 20-40 μm was noted. In another study, SF_6 was used to track air parcels in a seeded cloud, where milled salt particles were used as the seeding agent. In this study a broadening of the DSD was observed (Rosenfeld et al., 2010). Linking the evolution of cloud microphysical processes to hygroscopic seeding remains elusive despite worldwide hygroscopic cloud seeding experiments (Flossmann et al., 2019; Silverman 2003; Tessendorf et al., 2012). The major hurdle is that the physical processes leading to precipitation formation are dynamic and complex and difficult to directly and quantitatively track and link to the seeding (Tessendorf et al., 2012).

In the current study, using an mAMS, we demonstrate that the seeding signatures within stratus and convective clouds are detectable with an evidence-based approach without using tracer gasses. We further show that the seeding materials and the seeding-activated cloud droplets in convective clouds can propagate to higher altitudes while also modulating the cloud's microphysical properties. The ultimate goal is to investigate the microphysical pathways that are modified in cloud seeding operations. These experiments took place in the region near Solapur (17.66° N, 75.90° E),

India, during the Cloud-Aerosol Interaction and Precipitation Enhancement Experiment (CAIPEEX) (Prabha et al., 2011; Kulkarni et al., 2012; Prabhakaran et al., 2023) in 2019 (phase-IV).

2. Materials and Methods:

2.1 Measurements of cloud properties.

Three cloud seeding events carried out on 21 August, 23 August and 24 August in 2019, are selected here for evaluation of seeding signatures and plausible links to microphysical properties. Instruments for the measurement of flare particles, aerosol, and cloud properties were operated on a Beechcraft-B200 aircraft. This aircraft was equipped with flare racks located under both the wings and the belly. The flare racks in the wings are used for warm cloud seeding operations (Mather et al., 1997), while the belly is utilized for cold cloud seeding operations (French et al., 2018; Friedrich et al., 2020). The temperature (T, ºC), relative humidity (RH%), wind speed (ms^{-1}) and wind directions were measured with the Airborne Integrated Meteorological Measurement System (AIMMS-20). The DSD in the size range of 2-50 μm was measured with a Cloud Droplet Probe (CDP-2) manufactured by Droplet Measurement Technologies LLC, USA. The bulk microphysical properties are derived from the measured DSDs, e.g. the total number concentration (N_t, cm^{-3}) and liquid water content (LWC, g m^{-3}). The effective radius (r_e, μm) was calculated from the ratio between the third and second moments of the DSDs (Martin et al., 1994). The Precipitation Imaging Probe (PIP) was used to document drizzle drops in the cloudsover the size range of 100-6200 μm. The technical specifications of these instruments are shown in Table 1. The uncertainties associated with the CDP, and single particle light scattering instruments like the CDP, have been well characterized and documented (Baumgardner et al., 1983, 2001, 2016; Lance et al., 2010). In water droplets the sizing

uncertainty is ±20% and counting accuracy ±16%, which propagates into a LWC uncertainty of ±38%.

Cloud properties are altered by the entrainment of cloud-free air masses at the edges of the cloud; hence to minimize the influences of entrainment and mixing processes in the seeded and non-seeded clouds, only clouds with near adiabatic or slightly diluted cloud parcels are considered to evaluate cloud microphysical properties. Only cloud passes with LWC in the range of $0.75 < LWC/LWC_{max} < 1$ (Konwar et al., 2021) were selected for this study. Here, LWC_{max} represents the maximum measured value of LWC during a cloud pass. Note that this cloud regime may be considered as the cloud core, typically located within the strongest updrafts zone. Our main aim is to select the DSDs located within the cloud core regime. Note that in most naturally developing clouds the LWC_{max} values are less than the adiabatic LWC (LWC_{ad}) values because of the entrainment of drier air, mixing, precipitation fallout and radiative heating/cooling (Korolev et al., 2007). The maximum adiabatic fraction, $AF_{mx}=LWC_{max}/LWC_{ad}$, indicates the extent of dilution that has occurred in the cloud core regime. During their development and dissipation stages clouds undergo significant changes; therefore, it is practically impossible to find two clouds identical in all states, let alone their lifetimes. It is to be noted that the AF values may not accurately represent the mixing state when CC is significant and drizzle particles form within the clouds. Additionally, studies of the seeding effect using parcel model simulations without the inclusion of mixing processes indicates a significant change in the LWC profile compared to the non-seeded cloud (Konwar et al., 2023). Such changes in LWC values at different vertical distances from the cloud base of the seeded clouds do not necessarily imply the true dilution rate in the observations. Since the cloud seeding flare produces high concentrations of small-sized particles, they can be activated into cloud droplets in strong updraft regimes with high supersaturation (Konwar et al., 2023; Prabhakaran et al., 2023). In

a parcel model simulation, small aerosols released from flares are found to be activated due to an increase in supersaturation when the collision-coalescence process is active (Konwar et al., 2023). For details on the nucleation process within the zone of intense collision, where rapid decrease in drop concentration leads to an increase in supersaturation, readers are referred to Pinsky and Khain (2002). At a given height, however, seeding does not change the adiabatic value, but activation of new particles at a given level due to seeding can alter the AF. Another aspect is that near the cloud base the LWC_{ad} values are quite small (e.g., < 1 g m^{-3}), therefore any small change in the measured LWC could indicate a large change in AF. With this background information in mind, the DSDs for Seed Cloud (SCl) and No Seed Cloud (NSCl) conditions are compared at different vertical distances above the cloud base (D*, km). The lowest unbroken visible section of a convective cloud was selected as the cloud base. The cloud top is defined as the maximum altitude attained by these clouds at any given moment during their development.

Table 1

Details of Instruments used on the aircraft and for offline analysis in the study

Instrument	Variable	Range/Remark	Reference
Aventech AIMMS-20	GPS Coordinates, altitude above Mean Sea Level (MSL), temperature, dew point temperature, horizontal and vertical winds	Vertical wind accuracy 0.75 m s^{-1}	https://aventech.com/products/aimms20.html
DMT CDP2	Cloud droplet number concentration and size distribution	3.0 – 50.0 µm	https://www.dropletmeasurement.com/product/cloud-droplet-probe/
DMT PIP	Particle image	100 µm – 6.2 mm	https://www.dropletmeasurement.com/product/precipitation-imaging-probe/
CVI	Droplet/ice crystal residuals	Particle Cut size ~ 7µm	https://www.brechtel.com/product/aircraft-based-counterflow-virtual-impactor-inlet-system-cvi/

2.2 Measurement of hygroscopic flare particles by mAMS and Correcting time trends of slow-vaporizing species

We utilized a mAMS to analyze the chemical compositions of residual particles from cloud droplets, specifically to trace flare particles within the seed clouds. The CVI is manufactured by Brechtel Manufacturing Inc. (BMI, Model 1204, www.brechtel.com). The cloud droplets were passed through the CVI to obtain the droplet residual that were sampled by the mAMS. Through the use of inertial impaction, the CVI inlet allows cloud hydrometeors with aerodynamic diameters larger than a certain size to pass through, depending on the velocity of the counterflow. A warm, particle-free dry nitrogen gas is directed towards the inlet against the direction of the ambient air flow. This causes a separation of in the incoming free stream air, with particles >7 μm in the sampled air having enough inertia to penetrate the counterflow and join the sample flow. The CVI adjusted flow rates with its internal software based on true air speed (TAS) obtained from the AIMMS. The cut-size is a function of various factors, e.g., air pressure, air speed, and the average angle of attack, is known to have an uncertainty of approximately ±1 μm. The heated air evaporates cloud droplets and the remaining dried residuals enter the mAMS where their chemical compositions are classified. Details of the operational principles of the CVI can be found in Ogren et al., 1985; Ogren, 1987; Noone et al., 1988; Shingler et al., 2012; Golderger et al. 2020; and references therein.

The mAMS measured the residual particles with vacuum aerodynamic diameters of less than 1 μm, sampling through an aerodynamic lens. The aerosol sample stream is intermittently blocked to measure background signals. The aerosol signal is the difference between unblocked ("open") measurements and those obtained during the blocked ("closed") period. The mAMS sampled 10 seconds of closed signal for every 110 seconds of open. The heater, operated at 600 ^{o}C, vaporized the sample, electron impact ionized the vapors, and the resultant ions were extracted into the mass

analyzer for measurement of chemical composition and mass distributions (Jayne et al., 2000; DeCarlo et al., 2006; Canagaratna, et al, 2007; Drewnick et al., 2015; Giordano et al., 2018; Salcedo et al., 2006).

Ice Crystal Engineering (ICE) Inc. (USA) manufactured the hygroscopic flares used in this work. The flares were composed of an aggregated mixture of potassium perchlorate ($KClO_4$) and calcium chloride ($CaCl_2$) (Hindman, 1978; Bruintjes et al., 2012).

For non-refractory ambient aerosol species (i.e., NH_4, NO_3, SO_4) aerosol concentrations are obtained from the difference between the open and closed signals. The vaporization of non-refractory aerosol species at 600°C typically completes on the timescale of hundreds of microseconds, however, semi-refractory species such as metals and salts may take minutes to completely vaporize (Canagaratna et al., 2007; Salcedo et al., 2006).

As discussed below, the Cl, HCl, and K from the $KClO_4$ and $CaCl_2$ in flares is a semi-refractory species which exhibits slow vaporization. These slow vaporizing species were analyzed using only the open signals.The background signal was calculated from measurements obtained immediately before the cloud intercept of interest.

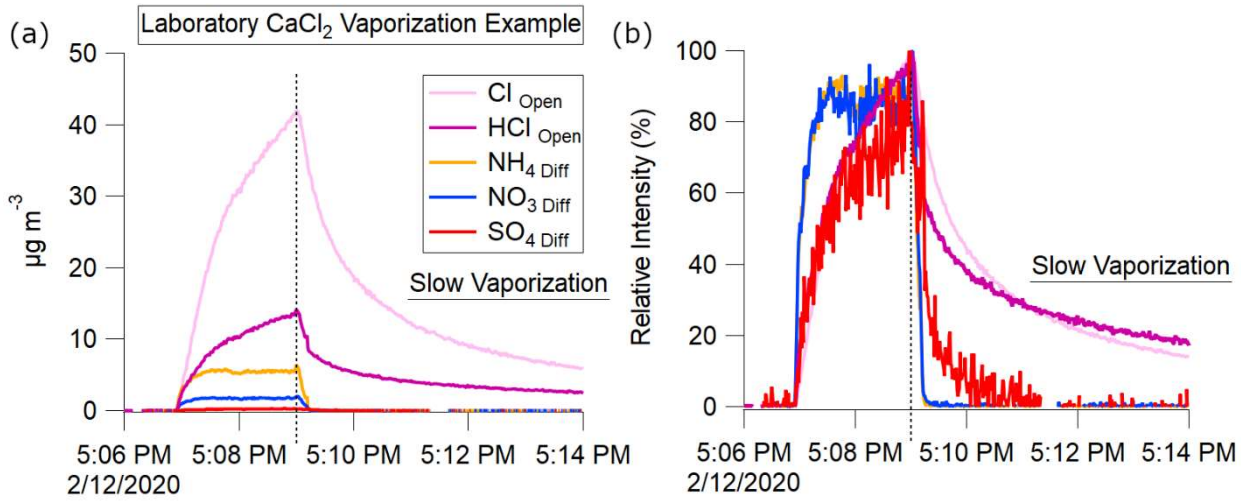

Figure 1. Laboratory atomized $CaCl_2$ AMS measurements observing slow vaporization of semi-refractory Cl species on 2/12/2020. Atomization begins at 5:07 PM ending at 5:09 PM. Slow vaporization is evident after 5:10 PM. The presence of NO_3, NH_4, and SO_4 are from calibration species (NH_4NO_3, NH_4SO_4) contaminants in the atomizer.

$CaCl_2$, the seeding component in the flares, has a melting point of 774 ºC. Laboratory measurements of atomized $CaCl_2$, primarily detected as Cl and HCl ions, exhibit the same slow vaporization seen in refractory salts (Drewnick et al., 2015). Fig. 1 shows a comparison of vaporization timescales of $CaCl_2$, NH_4NO_3, and $(NH_4)_2SO_4$ obtained with an AMS during laboratory measurements of $CaCl_2$ in solution with H_2O which had been atomized and passed through a drier before sampling. This behavior differs from that observed from non-refractory NH_4NO_3 and $(NH_4)_2SO_4$, which were present as tracers.

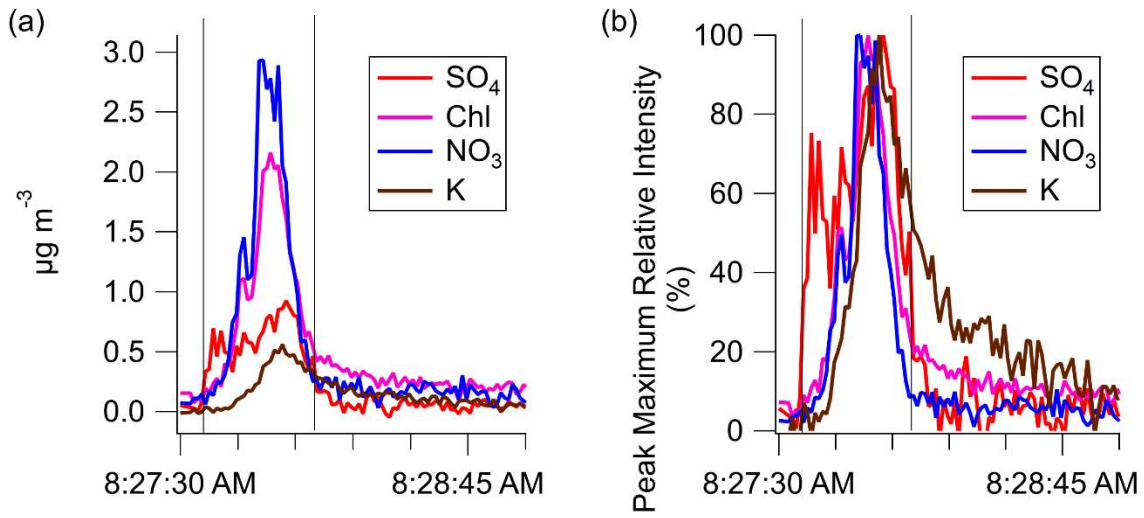

234

235 **Figure 2**. (a) shows the slowed time response of thespecies K and Cl for a seeded cloud pass on
236 August 23rd (b) the relative intensity with respect to peak maximum of each species highlights the
237 slowed decay of K and Chl compared to SO_4 or NO_3.

238 The seeded cloud pass shown in Fig. 2a illustrates a single seeded cloud pass. The K and Cl
239 time series have a delayed decay to background compared to sulfate or nitrate. The relative intensity
240 shown in Fig. 2b highlights the delayed response in the decay of the two flare associated species (K,
241 Cl).

242 An exponential decay was fit to each cloud intercept, from the signal peak to 5 e-folding
243 times. The average decay exponential(τ) for Cl, and K across all seeded cloud intercepts, is shown in
244 Table 2.

245

246

247

Table 2

Average decay time constants from seeded cloud intercepts during CAIPEEX- IV, 23 August 2019.

T	K	HCl	Cl
Mean	6.7	3.4	3.3
Std Dev	2.3	0.5	0.8

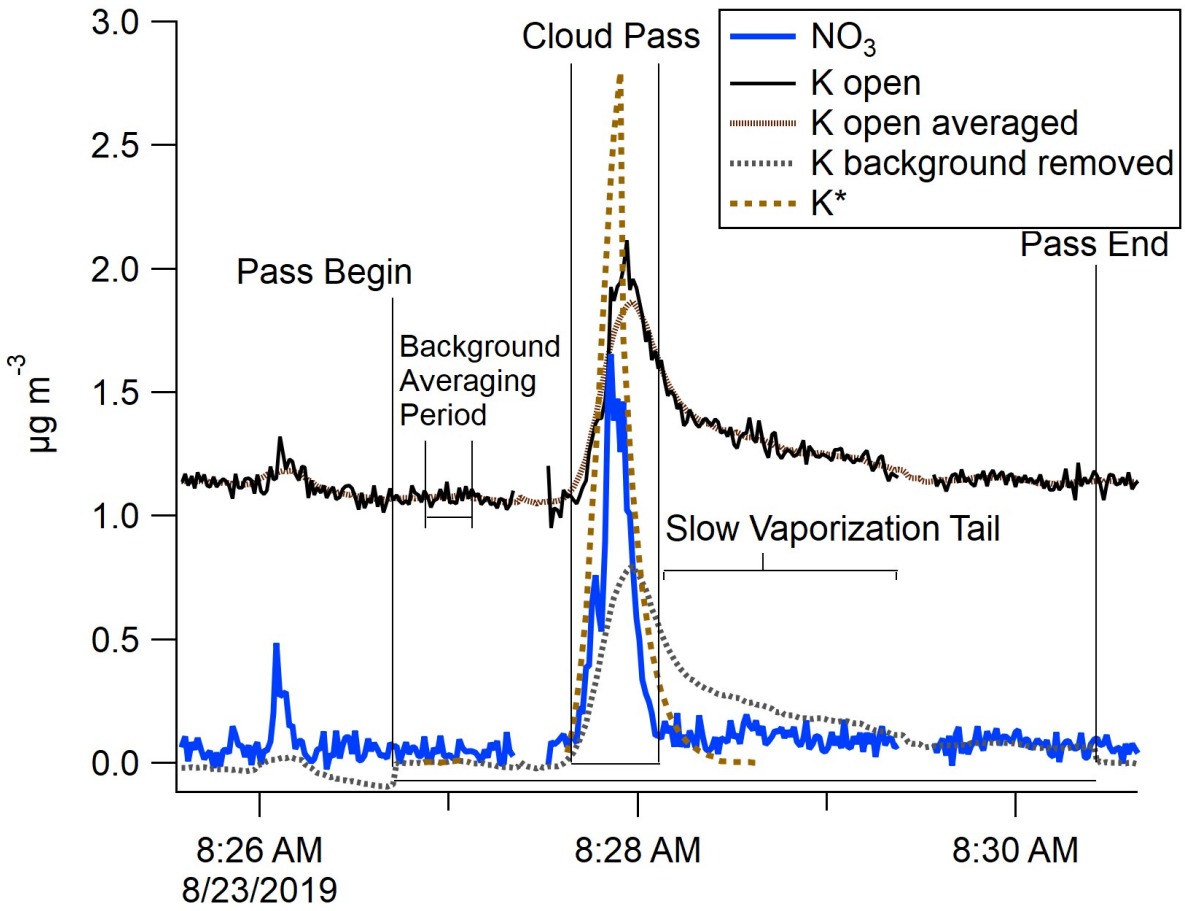

Figure 3. The measured semi-refractory open K signal and corrected K* signal from the mAMS are depicted for a seeded cloud pass on 23 August 2019. The periods from the beginning to the end of the cloud passes are also shown.

For each slowly vaporizing species, a new corrected time series was created. The start, stop, and maximum total mass times were identified for each cloud pass (Fig. 3). For each species, a background signal was determined from measurements during the non-cloud period preceding each pass. This background was subtracted from the signal observed during each cloud intercept.

The cloud intercept time series peakat the same time as the uncorrected series. However, the tails were corrected to decay within 5 tau e-folding times, while preserving the total mass. The equations used in these calculations are shown below.

The measured mass from the start of the pass to the end of the slow vaporization regime was scaled by the ratio of the total area divided by the area of fast vaporization (equation 1)

$$Conc._{Areacorrected}(t)\Big|_{End+(5\tau)}^{Start} = (Conc.(t) - Conc._{Background}) * \frac{Area_{Peak+Tail}}{Area_{Peak}} \quad (1)$$

The decay of this normalized mass is adjusted to the exponential decay fit (Table 2) to the slow vaporized mass (equation 2). This decay extends from the cloud pass peak to the end of the normal vaporization period plus five e-folding times (Giordano et al., 2018)

$$Conc._{TailCorrected}(t)\Big|_{End+(5\tau)}^{Peak} = Conc._{AreaCorrected}(t) * e^{(-\left(\frac{1}{\tau}\right)t)} \quad (2)$$

This decay-corrected time-shifted time series is normalized to the unmodified slow vaporizing total mass (equation 3)

$$Conc._{Corrected}(t)\Big|_{End}^{Start} = Conc._{TailCorrected}(t) * \frac{Area_{Peak}}{Area_{Peak+Are}{}_{Peak+Tail}} \quad (3)$$

Finally, we applied an enhancement factor correction to the mAMS data resulting from the ambient aerosol concentration being concentrated in the CVI by following Shingler et al., (2012).

3. RESULTS

3.1.1 Slow vaporization of semi-refractory seed aerosols

Although many aerosol species readily vaporize at 600 ^{o}C, some semi-refractory materials in nature do not. Submicron aerosol particles in the troposphere, that contain Cl, are rarely semi-refractory and vaporize quickly in the mAMS. However, Cl in seeded clouds was found to vaporize slowly. The Cl measured in clouds seeded using $CaCl_2$ and $KClO_4$ exhibited the same slow vaporization (Fig. 2) as Atomized $CaCl_2$ in the laboratory (Fig 1). The majority of atmospheric Cl-containing aerosols are non-refractory. In our study the slowly vaporizing Cl was only observed in seeded clouds; thus, we assume that the source of the slow vaporizing Cl was from the flare material. Aerosol K is uncommon except as super micron mineral dust. As shown in Fig.2b, slowly vaporizing signals of Cl and K were observed in the campaign during seeded cloud intercepts.

The combination of the isolation of cloud residuals by the CVI and the presence of K and semi-refractory Cl allow for discrimination of the particles containing the flare combustion products.

The element Ca, was also present in the flare. The boiling point of Ca of 1484 ^{o}C at ambient pressure means that this species was not vaporized inside the AMS and is thus considered a refractory species. Since Ca could not be observed in our study, the focus remained on the other species present.

As previously discussed, the time series of semi-refractory Cl and K signals are corrected to account for the difference in the decay response of slowly vaporizing species in the mAMS. Fig. 3 depicts the corrected (K*) and uncorrected semi-refractory K signals in the mAMS measurements for a seeded cloud pass, defining the periods for the start, peak, end, and tail of the pass.

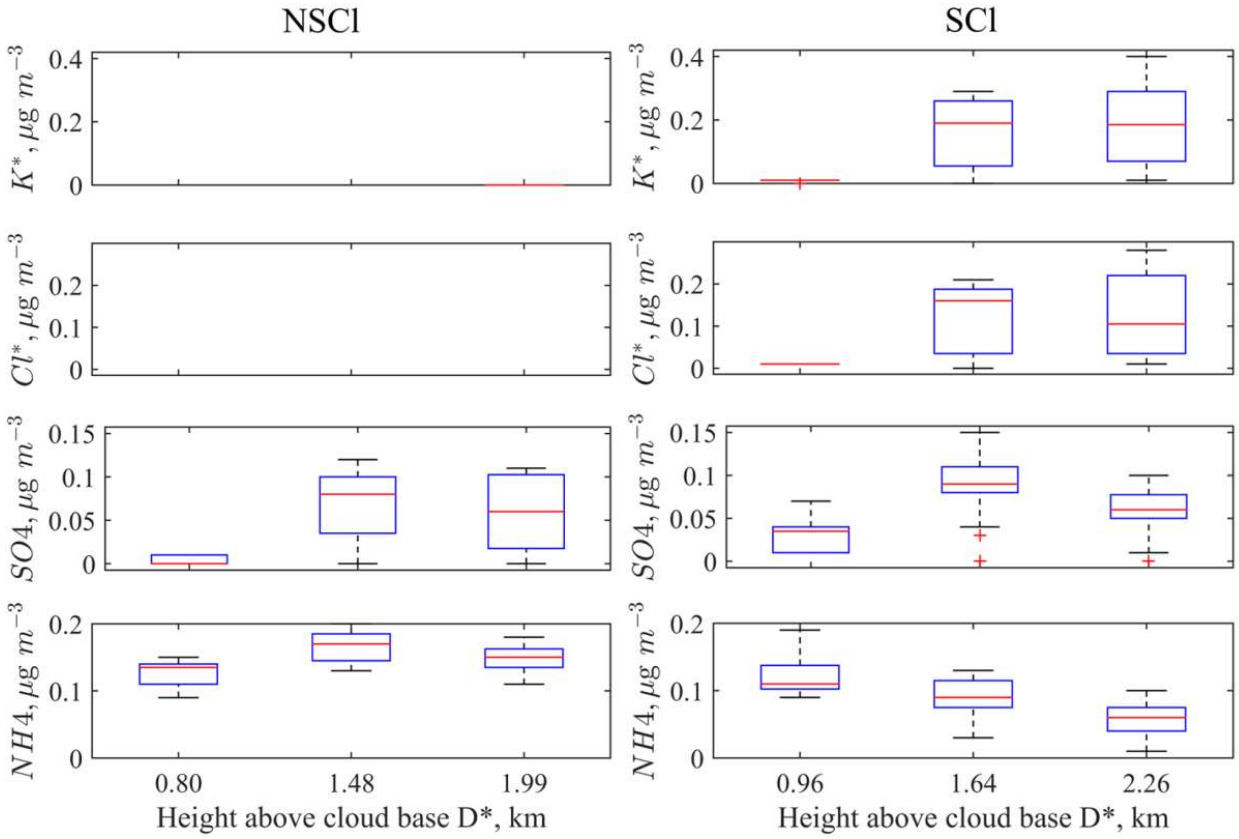

Figure 4. mAMS measurements of the mass concentrations of Cl^*, K^*, NO_3, and SO_4 versus D* (km) for cloud particle residuals from six cloud passes through the same cloud on 23 August 2019. The vertical profile box plots of each mAMS species at different altitudes shows median concentration and range (25-75th percentiles).Three non-seeded clouds (NSCl) and three seeded clouds (SCl) are shown.

A vertical profile of cloud residual aerosols, within the same cloud, taken before and after seeding, provides a platform for measuring and observing cloud physical and chemical changes. The resultant mAMS measurements from one such experiment, on August 23, 2019, with three cloud passes of the same cloud before and three passes after seeding are shown in Fig 4.

In the mid level, all chemical species were found in higher quantities in the seeded cloud than in the non-seeded cloud. Cl and K concentrations were significantly increased for all seeded cloud passes compared to non-seeded cloud passes. The measurement of the flare chemical species in the seeded cloud indicates that the mAMS could successfully identify the cloud droplets that containing seeding material.

An additional observation is the increased NO_3 and SO_4 concentration in the cloud drops of seeded clouds at upper heights. We hypothesized that the increased concentrations of these two chemical species could be linked with the activation of the flare particles and other organics while mixing with the naturally available NO_3 and SO_4 aerosols. The increased concentration of NO_3 in the seeded cloud may also be due to the presence of more LWC. The additional water drives nitric acid (HNO_3) from gas to liquid NO_3 (Wang and Laskin, 2014).

This example highlights the ability of the mAMS to identify flare associated species, by both increased concentration and time response, in order to confirm the presence of seeding material in cloud droplet residual.

3.2 Seeding experiment, Seeding Signature, and Cloud properties

3.2.1. Case i: 21 August 2019. The flight pattern of the aircraft during the cloud seeding experiment conducted on 21 August 2019 in a warm stratus layer is shown in Fig. 5a. The objective

was to identify the seeding materials and record the cloud microphysical properties. The wind direction was north-westerly at an altitude of nearly 4.10 km with a mean wind speed of 7 ms^{-1}. Cloud passes (T=5.14 ºC, H=4.39 km) were made through the stratus layer before the dispersal of seeding materials. Four hygroscopic flares were burned, two at a time, inside the layer cloud, from 8:01-8:08 UTC at H=4.10 km. Weak updrafts (W=0.61±1.53 m s^{-1}) prevailed indicate that the flare material might have drifted horizontally. Increased mass concentrations of K* and Cl* are noted in the downwind after the dispersal of the seeding agents, as shown in Fig. 5b and 5c. Repeated crosswind cloud passes at a similar level (T= 6.44 ºC, H= 4.10 km) were made downwind of the seeding. The aircraft could release non-volatile and fine aerosol particles through exhaust emission (Anderson et al., 1998), which may also contaminate the cloud mass. Prabhakaran et al. (2023) measured aerosol size distribution of background airmass, and then the background with aircraft exhaust during CAIPEEX. They reported that the aircraft exhaust can impact mean radius, spectral width and number concentrations of different modes of log-normal aerosol size distribution (see the supplementary materials at https://doi.org/10.1175/BAMS-D-21-0291.2). Solution of simple advection equations indicates dispersal of seeding plumes in the downwind region after nearly 3 minutes (not shown here) where the aircraft also recorded enhanced concentrations of K^* and Cl^*. Gayatri et al., (2023) illustrated the seeding impact downwind of the seeded area through the high-resolution numerical model in similar monsoon environment with the monsoon low-level jet (LLJ) as detailed in the present study. The cloud bases are situated very close to the region with high wind speeds in the monsoon low-level jet and the advection of seeding plume downwind of the seeded location is noted. However, the fact that seeding was done specifically in the strong updraft zones and the seed particles were also lifted inside the cloud and more cloud droplets were noted both in the observations and simulations. Earlier, during the Seeded and Natural Orographic Wintertime

353 Clouds: The Idaho Experiment (SNOWIE) (Xue et al., 2022) noted seeding plumes dispersed within
354 orographic clouds in more than 1 hour along the slanted downwind direction.

355

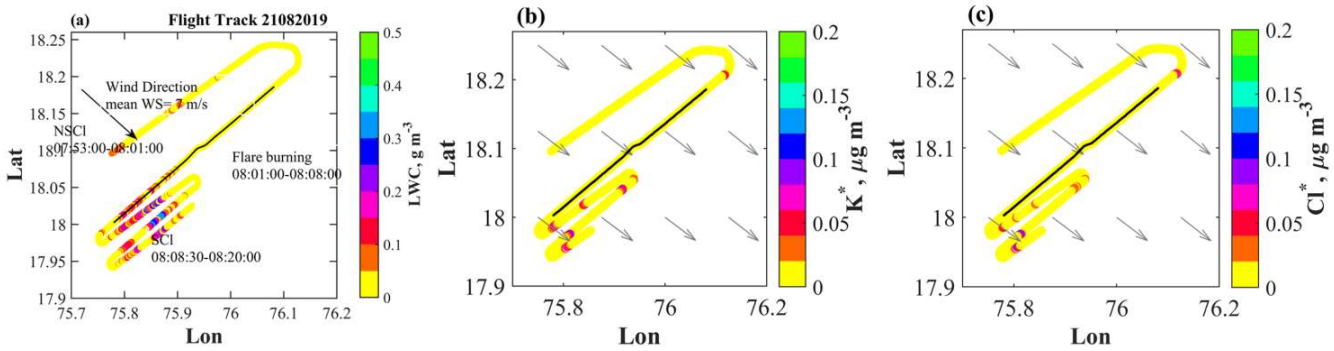

356

357 **Figure 5**. (a) The flight path during the seeding experiment on 21 August 2019 color coded by LWC
358 at 1 Hz resolution. Periods during which cloud measurements were made for non-seeded clouds
359 (NSCl) and seeded clouds (SCl) are annotated. Mass concentrations of (b) K^* and (c) Cl^* during the
360 seeding experiment are shown along the flight track. The ambient wind fields shown as arrow
361 obtained from https://cds.climate.copernicus.eu/ (0.25 ºX0.25 º), which are resampled to 0.125 º X
362 0.125º. A small area of elevated K and Cl, prior to the flare burning is noted. This was measured
363 outside the cloudy region as suggested by the LWC values and it might be appeared probably due to
364 other unknown sources.

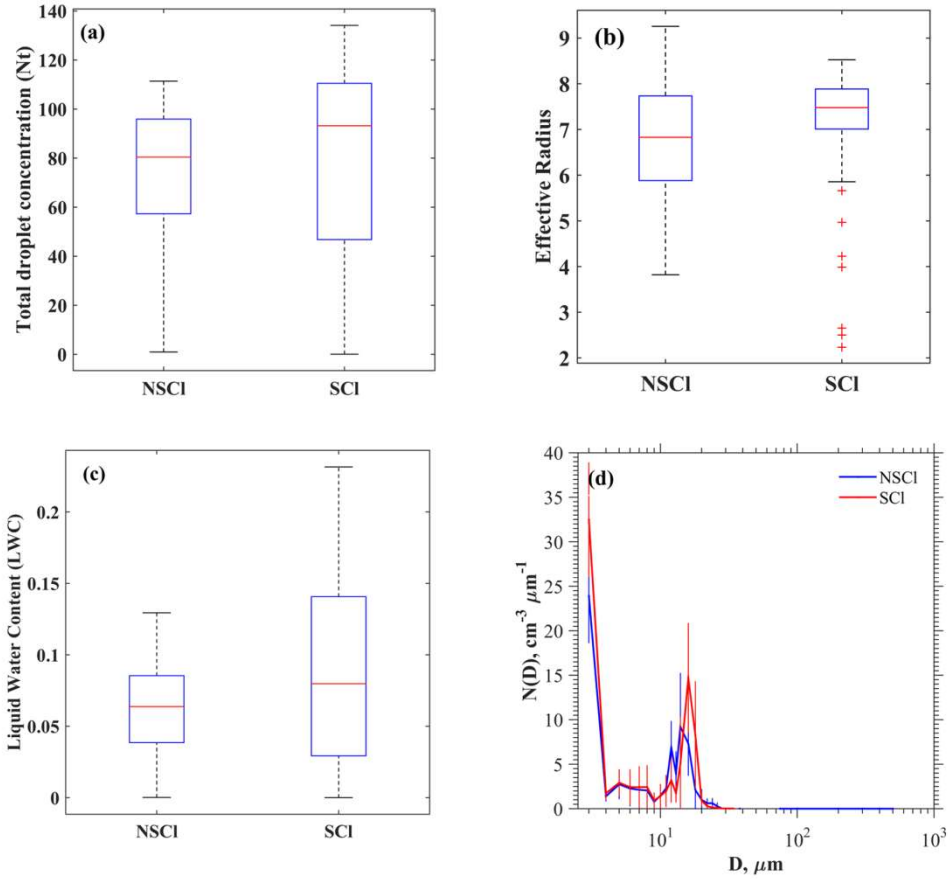

365

366 **Figure 6**: Box plots of (a) total droplet concentrations, (b) Effective radius, (c) LWC are shown for
367 NSCl and SCl. (d) Mean cloud DSDs with standard deviations (vertical bars) are depicted indicating
368 the variability. The selected DSDs fall within the criteria of $0.75 < LWC/LWC_{max} < 1$.

369 Stratus cloud passes were selected for study based on two criteria: a cloud pass duration
370 greater or equal to 5 seconds and N_t>10 cm^{-3}. Two NSCl cloud passes made during 7:53:00-7:53:31
371 UTC and 7:55:17-7:55:41 UTC were chosen for the analysis. After the flares had dispersed, three
372 passes during 08:08:37-08:08:45 UTC, 8:09:42-8:09:53 UTC, and 8:09:59-08:10:39 UTC were
373 selected based on the elevated levels of detection of K and Cl (see Fig. 5b and 5c). Box plots of N_t,
374 r_e and LWC are displayed for NSCl and SCl in Figs. 6a, b and c, respectively. It is worth noting that
375 the SCl cases exhibit greater median values for these three parameters. The properties of DSDs along

the cloud pass are shown in Supplementary Figs. S1 and S2. The DSD properties and mass concentrations of K* and Cl* are provided in Table 3. Increased droplet concentrations in the smallest size bin are noted after a few minutes from the seeding time while drizzle drops were not observed in the SCl. Comparsions are made for mean SCl-DSD and NSCl-DSD in the range $0.75<LWC/LWC_{max}<1$, as illustrated in Fig. 6d. An increase of N(D) at D ≈ 3 μm and in the size range 13 < D < 20 μm are noted in the SCl, while N(D) decreased in the size range 4 < D < 13 μm. The increase in the smallest cloud droplets may be due to freshly nucleated aerosols, likely due to the activation of seeding materials. The increase in the mid-size droplet concentrations could be due to the activation of coarse mode aerosols and subsequent diffusional growth. Since drizzle drops were not formed, it may suggest that hygroscopic seeding in stratus cloud with low LWC value e.g. < 0.5 g m^{-3} may not yield a significant positive seeding effect for the production of drizzle.

3.2.2 Case ii: 23 August 2019.

Fig. 7a depicts the flight patterns for the case on 23 August 2019. This seeding event is selected for evaluation because (i) The SCl and NSCl convective clouds were isolated and in the growing and non-precipitating stages, (ii) the cloud top was below freezing level (5 km) therefore ideal for studying warm rain microphysics, (iii) The SCl and NSCl were formed within the same area (20 km x 20 km) and lastly, (iv) both the SCl and NSCl grew to similar cloud top altitudes (≈4 km), therefore roughly at similar growth stages. These conditions made this case suitable for evaluating the seeding effect on warm rain. The cloud base height over the observational area was nearly 1.80 km. Northwesterly winds (mean wind speed of 12 ms^{-1}) prevailed in the boundary layer at 1.30 km (850 mb). Before the dispersal of flare materials at cloud base, the cloud microphysical properties of NSCl were measured from 7:49 to 8:06 UTC by step-wise multiple cloud penetrations from the top

399 (≈ 3.90 km) to near the cloud base (≈ 1.80 km). A maximum updraft of 4.40 ms^{-1} was observed at
400 the cloud base. After completion of NSCl measurements, the aircraft then circled below the cloud
401 base and burned four hygroscopic flares (two on each wing) in the updrafts during 8:08-8:12 UTC,
402 followed by several step-wise cloud penetrations at nearly 1000 ft intervals, from near the cloud base
403 to cloud-top during the period 8:14-8:28 UTC.

404 The profiles of N_t and r_e *w.r.t.* the D*s are shown in Fig. 7(b,c). The mass concentrations of
405 K* and Cl* corresponding to N_t and r_e, respectively, are also indicated. The statistical properties of
406 the DSD parameters are presented in Table 3. The variations of DSDs along the cloud transects,
407 values of r_e, drizzle concentration, LWC, and W are shown in the supplementary material's Figs. S3-
408 4. Note that the SCl and NSCl were not identical due to the natural variability discussed previously,
409 with this background the following observations are noted:

410

411

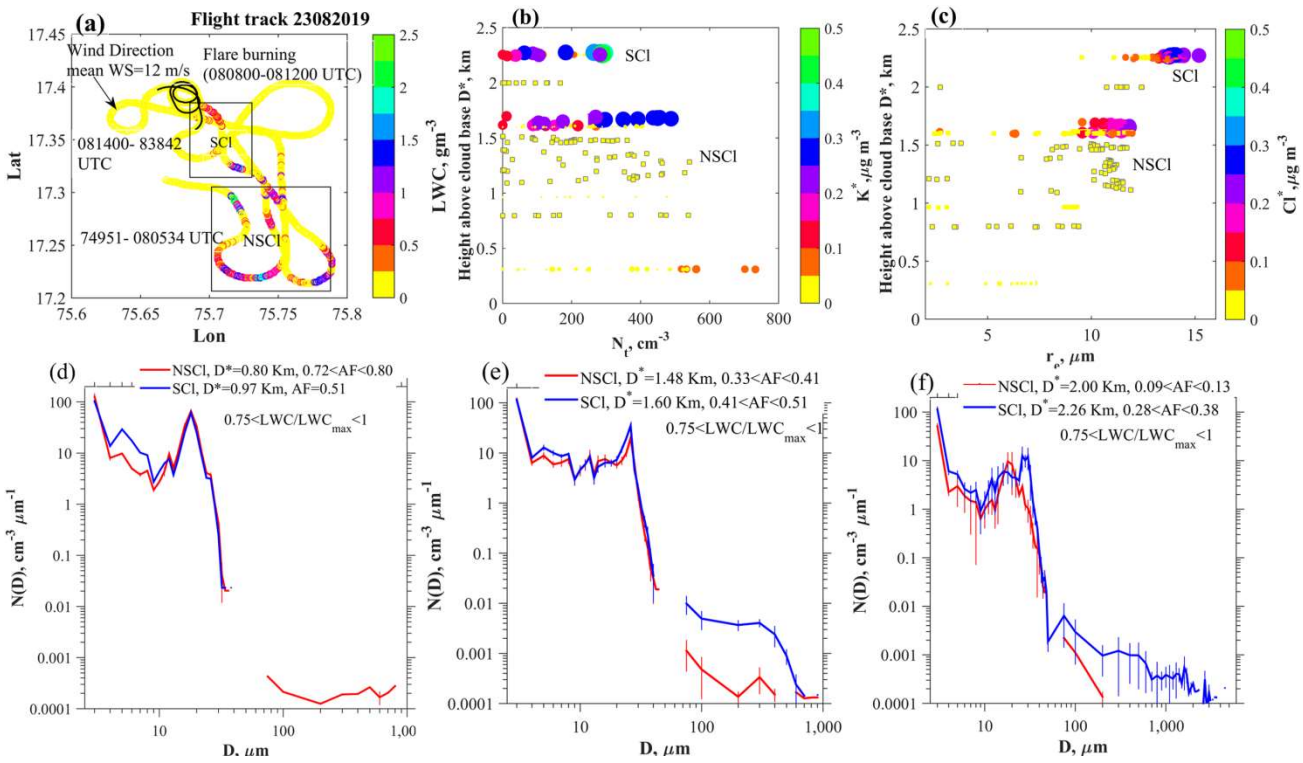

Figure 7. (a) Flight track during the seeding experiment on 23 August 2019. The flight track during the flare burning period is overlaid with black color. The areas of seeded cloud (SCl) and non-seeded cloud (NSCl) are indicated on the figure panels. The arrow indicates the wind direction near the cloud base height of 1.80 km. The color bar indicates the liquid water content (LWC, gm^{-3}) of clouds. Profiles of (b) N_t, (cm^{-3}) and (c) r_e, (μm) *w.r.t.* height above cloud base, D* (km) are shown. The parameters are indicated in the color bars with the mass densities of K* and Cl*, (μg m^{-3}). The squares with black edges indicate NSCl, while filled circles indicate SCl. The sizes of the symbols increase with increasing mass of the chemical components. Mean cloud drop size distributions with standard deviations indicated by the error bars of slightly diluted clouds ($0.75<LWC/LWC_{max}<1$) at various D* (km), for NSCl and SCl, (d), (e) and (f).

425 Table 3.

426 Cloud properties of Non-Seeded Cloud (NSCl) and Seeded Cloud (SCl) along the cloud transect are
427 shown. Vertical distance above the cloud base (D*, km), Mean values and standard deviation of total
428 droplet concentration N_t, (cm^{-3}) in the diameter range 2-50 μm, maximum droplet concentration
429 (N_{tmax}, cm^{-3}), mean effective radius (r_e, μm), liquid water content (LWC, gm^{-3}), Maximum LWC
430 (LWC_{max}), maximum adiabatic fraction (AF_{mx} = LWC_{max}/LWC_{ad}), where LWC_{ad} is the adiabatic
431 LWC calculated from a parcel model. AF_{mx} for layer clouds on 21082019 is not calculated. The
432 mean of small droplet concentration (D<11 μm) and the maximum of small droplet concentration,
433 and drizzle concentration (DrizzleCon, (cm^{-3}) are also shown. Concentrations of K* and Cl* in μg m^{-3}
434 during NSCl and SCl observations are indicated. Due to limited field calibrations, the
435 concentrations presented here are nitrate equivalent. Below Detection Limit (BDL) data are
436 indicated.

Case	D* (km)	N_{tmn} ±SD (cm^{-3})	N_{tmax} (cm^{-3})	r_e ±SD (μm)	LWC ±SD (gm^{-3})	LWC_{max} (gm^{-3})	AF_{mx}	N_{tmn}, [N_{tmx}] (D<11μm)	DrizCon ±SD (cm^{-3})	Mean K* ±SD [K^*_{Max}] mg m^{-3}	Mean Cl* ±SD [Cl^*max] mg m^{-3}
2108-NSCl	0.35	73±23	105	7.28±1.22	0.07±0.03	0.13	-	46±20[89]	0	BDL	BDL
2108-NSCl	0.40	73±35	111	5.93±1.03	0.05±0.03	0.13	-	39±20 [77]	0.004±0.02	BDL	BDL
2108-SCl	0.07	47±40	108	7±1.50	0.05±0.05	0.13	-	21±16 [49]	0±0	0.0024±0.001 [0.004]	0.003±0.0005 [0.004]
2108-SCl	0.08	62±40	111	6.05±1	0.05±0.04	0.10	-	42±28 [80]	0±0	0.06±0.03 [0.09]	0.02±0.02 [0.06]
2108-SCl	0.08	92±35	134	7.54±0.86	0.11±0.06	0.23	-	44±17 [79]	0±0	0.003±0.004 [0.02]	0.0005±0.0003 [0.001]
2308-NSCl	1.99	65±60	167	10.72±2.86	0.19±0.17	0.48	0.13	30±27 [68]	0±0	BDL	BDL
2308-NSCl	1.48	177±104	360	9.70±2.42	0.42±0.34	1.11	0.41	101±57 [185]	0.01±0.01	BDL	BDL
2308-NSCl	1.33	254±173	541	10.26±1.31	0.69±0.48	1.57	0.61	121±84 [262]	0.01±0.01	BDL	BDL
2308-NSCl	1.16	254±184	528	9.40±3.22	0.80±0.66	2.00	0.88	116±75 [210]	0.31±2.65	BDL	BDL
2308-NSCl	0.80	208±198	538	6.57±2.60	0.32±0.44	1.22	0.80	107±84 [221]	0.05±0.04	0.001±0.0005 [0.001]	BDL
2308-SCl	0.31	402±194	733	6.74±0.84	0.42±0.22	0.69	0.92	144±69 [323]	0±0	0.03±0.22[0.08]	0.014±0.01 [0.02]
2308-SCl	0.31	236±192	482	5.90±1.64	0.23±0.20	0.54	0.72	90±67 [169]	0±0	0.004± 0.003 [0.01]	0.0005± 0.0002 [0.0008]
2308-SCl	0.96	186±158	477	7.30±3.01	0.35±0.31	0.97	0.51	81±71 [196]	0.002±0.007	0.005±0.001 [0.008]	0.011±0.003 [0.015]
2308-SCl	1.64	200±139	488	10.41±1.50	0.62±0.51	1.74	0.57	83±53 [198]	0.53±0.50	0.17± 0.10 [0.29]	0.12± 0.08 [0.21]
2308-SCl	1.60	162±120	332	9.70±3.00	0.50±0.38	1.04	0.34	71±54 [157]	0±0	0.003±0.001 [0.005]	0.003± 0.001 [0.004]
2308-SCl	1.60	184±139	404	9.50±2.82	0.57±0.58	1.55	0.51	95±63 [183]	0.41±0.43	0.01± 0.01 [0.02]	0.023±0.02 [0.08]
2308-SCl	2.26	175±107	320	13.10±1.14	0.80±0.50	1.49	0.38	83±51 [155]	0.43±0.52	0.18±0.12 [0.40]	0.11±0.10 [0.28]
2408-NSCl	0.21	92±92	244	5.55±1.76	0.06±0.06	0.18	0.31	56±59 [147]	0±0	0.0008±0.003 [0.001]	0.002±0.002 [0.005]
2408-SCl	0.20	159±153	413	5.57±1.76	0.14±0.15	0.41	0.70	65±57 [157]	0±0	0.002±0.001 [0.003]	0.001±0.001 [0.002]
2408-SCl	0.20	161±189	649	5.91±2.06	0.16±0.18	0.56	0.96	70±88 [321]	0±0	0.01±0.01 [0.02]	0.004±0.003 [0.01]
2408-SCl	0.20	300±171	603	6.58±1.30	0.32±0.19	0.54	0.93	111±72 [347]	0±0	0.02±0.01 [0.05]	0.01±0.01 [0.02]

437

(i) At nearly D* = 0.96 km, smaller mean concentrations of N_t (186±158 cm^{-3}) are noted for SCl compared to the NSCl (N_t = 208±198 cm^{-3}) cloud pass at D* = 0.80 km. At these two nearly similar levels, the mean r_e values for the SCl case (r_e = 7.30±3.01 μm) were greater than those for the NSCl case (r_e = 6.57±2.60 μm). At greater D* of 1.60 km (r_e = 9.50±2.82 μm) and 2.26 km (r_e=13.10±1.14 μm), drizzle drops (see Table 3) were noted in the SCl cases. This may indicate active CC process in the SCl case. The mean DSDs are shown in Fig. 7(d,e) selected considering the criteria $0.75 < LWC/LWC_{max} < 1$ of the cloud transects. The corresponding AF values indicated on the panels suggest active entrainment and mixing processes in these clouds. The production of drizzle in some of the clouds may also lower the AF values which means that the dilution rate is not accurate in such clouds. The seeding effect may give rise to the initial production of drizzle particles, which were seen within the tail of the DSDs. Hence, the tail effect of the seeding particles appears to be active. Note that since the cloud passes were made in the developing stage of the cloud, these drizzle drops were formed spontaneously, not falling from the cloud tops because their terminal velocities are less than the updraft velocities. The broadening of the DSDs will serve to further increase the efficiency of the CC process (Andreae, et al, 2004; Rosenfeld et al., 2008; Rosenfeld et al., 1994; Freud et al., 2012; Konwar et al., 2012) leading to the production of drizzle drops at higher D*s. Also, stronger updrafts (≈ 5 ms^{-1}) were observed in SCl (see Fig. S4n), which helped in the growth of larger-sized droplets.

The formation of drizzle drops (D>100 μm) in the SCl was noted (Fig. 7(e,f) and Fig. S4) while no significant drizzle concentrations were noticed for NSCl (Fig. S3). The difference in drizzle concentration suggests that the flare particles modulate the mid-size cloud droplets (D ≈ 14 μm) that grow further by diffusion process. As the drizzle drops fall under the influence of gravity, stronger downdrafts are most likely due to the cooling by evaporation (see Fig. S4n). Moreover, small

droplets of D≤11 μm were observed at high altitudes for both clouds (Table 3). The scatter plots between r_e-K^* and r_e-Cl^* are shown in Fig. S5. The prevailing dynamical conditions e.g., vertical velocity are also indicated. It is found that the larger sized droplets (greater r_e values) are associated with the larger mass concentrations of K^* and Cl^*, in the SCl. In both the updrafts and downdrafts, all these chemical species were present. Having found the seeding tracers Cl^* and K^* at different altitudes, it may be emphasized that the modification of cloud properties occurs due to the dispersal of seeding particles through the cloud base. Seeding particles were present at deeper D*s as the cloud droplets were transported through updrafts and re-circulated as the cloud developed (Khain et al., 2013).

It is important to note that the differences in cloud microphysical properties observed between the seeded and unseeded clouds could be a result of natural variability, and more data are needed to arrive at a statistically significant result. However, given that these differences were accompanied by statistically different concentrations of chemical composition in the cloud droplet residues in the same environmental conditions, the evidence is compelling that seed material has a) transported to altitudes above the cloud base where they were released and b) these aerosol particles have influenced cloud microphysical processes.

3.2.3 Case iii: 24 August 2019.

The third cloud seeding case was carried out on an isolated convective cloud. The flight path is shown in Fig. 8a. South-westerly winds with a mean speed of 9 m s^{-1} were noted near the cloud base at 2.1 km with a maximum updraft of 8 m s^{-1}. One cloud pass before the flare dispersal was made from 08:55-08:59 UTC above the cloud base at ≈ 2.3 km. Three downwind cloud passes during

09:05-09:07 UTC were made at ≈ 2.3 km after the flares were burned. The variations of N_t, and r_e *w.r.t.* D* are shown in Figs. 8b,c. Increased mass concentrations of K^* and Cl^* are noted in SCl cases that identify the seeded clouds. The DSD properties of the clouds are shown in supplementary Fig. S6 & S7 and their parameters are indicated in Table 3. The mean DSDs (Fig. 8d) indicate increased droplet concentration in the small and mid-drop diameter ranges. Note that the AF values indicated strong dilution in the NSCl DSDs, which may also impact the observed differences in the droplet number densities. No marginal increment in r_e values was observed in the SCl. Another aspect to consider here is the effect of strong updraft of 8 m s^{-1}. Using the Twomey (1959) equation the maximum droplet concentration formed in an updraft (W) can be expressed in terms of W and CCN-SS spectra, i.e. $N_{CCN}=C\,SS^k$ i.e. (Roger and Yau, 1989),

$$N \approx 0.88\, C^{2/(k+2)}\left[7\, X\, 10^{-2}\, W^{3/2}\right]^{k/(k+2)} \qquad (4)$$

Here, W is in cm s^{-1}, $N_{CCN}= 799\ SS^{0.43}$, which is obtained from the CCN counter (Roberts and Nenes, 2005; Nenes et al., 2001 and reference therein) operated in the research aircraft. During the cloud passes, maximum updrafts of W= 2.89 m s^{-1}, 1.00 ms^{-1} and 1.91 m s^{-1} were obtained. These values suggest that droplets formed in these updrafts could be 593 cm^{-3}, 448 cm^{-3} and 531 cm^{-3}, respectively. If we use the maximum updraft speed of 8 ms^{-1} measured below cloud base, the droplet concentrations formed in this updraft could be as high as 777 cm^{-3}. In this scenario, the supersaturation could be greater than 1%, which can activate small-sized CCN. Therefore, the presence of strong updrafts that yield high SS could be one reason for the increasing N_t in the seeded clouds; while dry air mixing in the NSCl cases could be another reason for the smaller concentration of N_t. These processes may be attributed for the change in LWC values in the SCl cases.

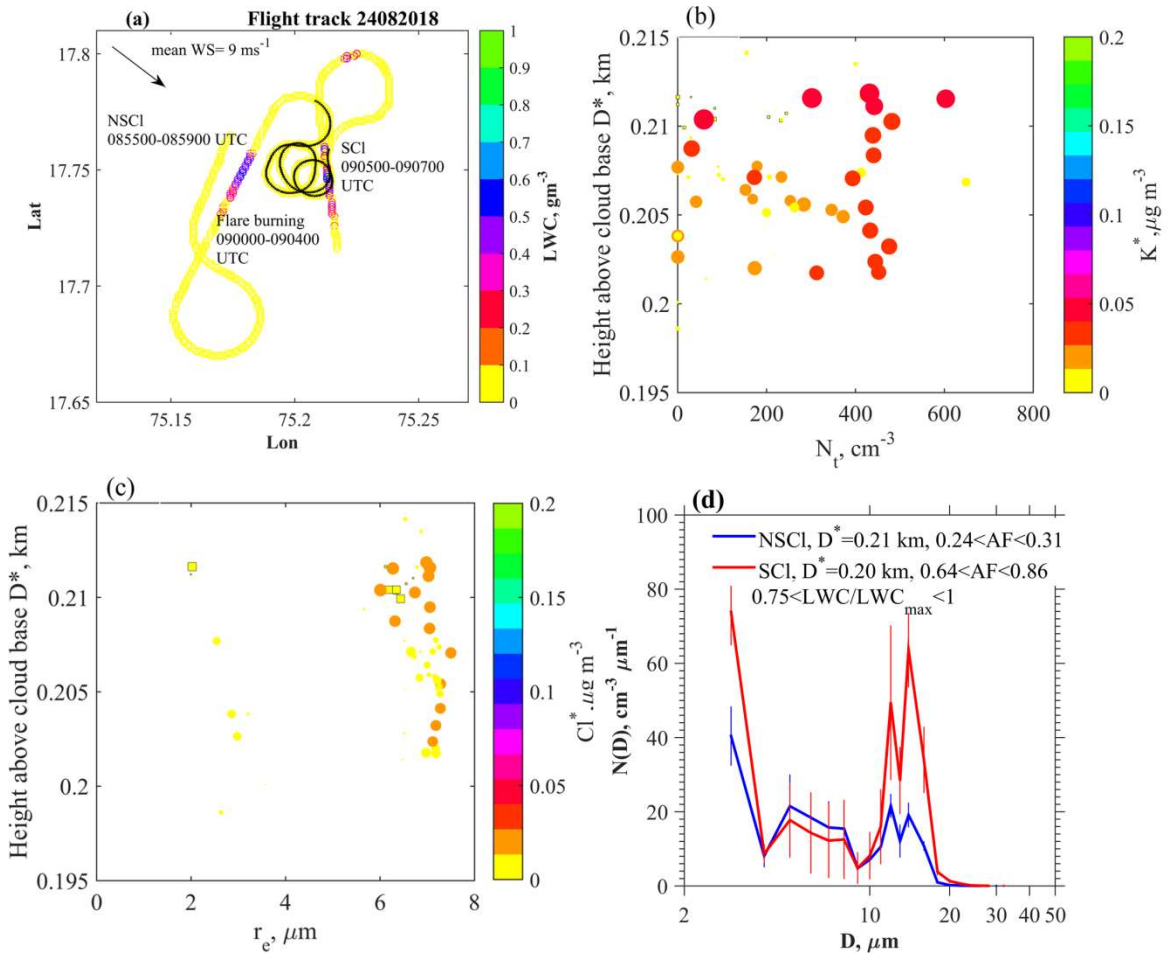

Figure 8. (a) Flight path during the seeding experiment on 24 August 2019. Periods during which cloud measurements were made for NSCl and SCl are indicated. The black line indicates the flare burning. Profiles of (b) N_t, and (c) r_e, *w.r.t.* D* (km). The parameters are indicated with the mass concentrations of K^*, (μg m^{-3}), and Cl^* (μg m^{-3}). (d) Mean DSDs with standard deviations indicated by the vertical bars, of clouds ($0.75<LWC/LWC_{max}<1$) above the cloud base, for NSCl and SCl. The adiabatic LWC fractions corresponding to the DSDs are also indicated.

4. Summary and conclusions:

The successful identification of seeded cloud hydrometeors, and the tracing back to their seeding origins in cloud seeding experiments has been an outstanding challenge for cloud seeding operations. The unequivocal identification of seeding material within clouds was the primary difficulty in such experiments. During the CAIPEEX 2019 seeding experiments conducted in India, we measured cloud microphysical properties and traced the seeding material with an mAMS behind a CVI in convective and stratus clouds.

In our experiments, the mAMS identified an enhancement of both K and Cl mass concentrations, most likely from the oxidizing agent (KClO) and seed material ($CaCl_2$). In stratus and convective clouds, such enhanced concentrations of refractory K and Cl should be considered as a seeding signature.

Enhanced small-sized droplet concentrations that were measured near the cloud base of convective clouds and in a warm stratus layer are noted. This result indicates that during the monsoon season with an available moisture supply, even the small-sized CCN present in the seed material could be activated into cloud droplets. The presence of strong updrafts near the cloud base of isolated convective clouds could also play a major role in the activation of small-sized CCN to cloud droplets. These strong updrafts would yield high supersaturation values, thus activating small-sized CCN. The impact of strong updrafts on the activation of cloud droplets, especially when seeding agents are dispersed below the cloud base, requires more focused attention and study.

In the case of a convective cloud, clear differences in the cloud microphysical properties of SCl compared to NSCl are noted. The flare materials released below the cloud base were lifted to a height of 2.25 km above the cloud base. In the lower part of the SCl larger droplet concentrations

were noted. The SCl also had a larger r_e than the NSCl at similar heights above the cloud base. The seeded clouds contained more drizzle drops, suggesting that they reached the threshold for warm rain initiation at a lower distance from the cloud base than the non-seeded clouds. These results from the limited sample indicate the plausible tail effect of the largest particles in the flares, initiating large cloud drops and drizzle. Though this case study indicate the importance tails effect; conclusive evidence would require much more data.

Whether competition or the tail effect is important in a successful cloud experiment remains to be examined, as the prevailing dynamical conditions can play a significant role in controlling the cloud microphysical processes. These complexities need to be addressed with more experiments using mAMS.

This study identifies a novel methodology to simultaneously track and measure the cloud seeding signatures and to assess how the seeding alters the microphysical properties of clouds leading to raindrop formation. The utilization of an mAMS in cloud seeding experiments together with a CVI allows for identifying the seeded cloud parcels of interest, leading to a better understanding of the effects on the microphysical properties of the cloud. Although these measurements of flare material in seeded clouds are associated with changes in physical properties, the data set is too limited to unequivocally assert that this methodology will always be successful. Future studies with a much larger data set will provide more statistical evidence linking seed aerosol and increases in precipitation.

Acknowledgment: Indian Institute of Tropical Meteorology, Pune and the CAIPEEX project are funded by the Ministry of Earth Sciences, Govt. of India. We thank Director, IITM for continuous supports. The authors are grateful to the team members, the ground staff, V. Ruge and S. Patil of

M/S Tesscorn AeroFluid, Inc., and the pilots for their dedicated efforts in conducting the project. The authors are grateful to the Editor and two anonymous reviewers for their insightful suggestions that helped improve the manuscript.

Data availability

mAMS and Cloud data are available at:
https://iitmcloud.tropmet.res.in/index.php/apps/files/?dir=/&fileid=59847#

Author contributions

TP and DW designed the mAMS experiment; MK, BW and ECF prepared the initial draft; KH, MK, BW, ECF, SC, SB, NM, MV, SJ and TP participated in the aircraft experiment; DB, TP, DW, DA, PM, MK, BW, ECF, MV, SC,SB and SAD reviewed the manuscript. All authors agree with the final version of the manuscript.

Competing interests

The contact author has declared that none of the authors has any competing interests.

References:

Anderson, B. E., Cofer, W. R., Bagwell, D. R., Barrick, J. W., & Hudgins, C. H.. Airborne observations of aircraft aerosol emissions I: Total nonvolatile particle emission indices. Geophysical Research Letters, 25, 1689–1692, 1998.

Andreae ,M. O., Rosenfeld, D., Artaxo, P., Costa, A. A., Frank, G. P., Longo, K. M., and Silva-Dias, M. A. F.: Smoking rain clouds over the Amazon, Science, 303, 1337–1342, 2004.

Baumgardner, D.,**:** An analysis and comparison of five water droplet measuring instruments. *J. Appl. Meteor.*, 22, 891-910, 1983.

Baumgardner, D., H. Jonsson, W. Dawson, D. O'Connor and R. Newton. : The cloud, aerosol and precipitation spectrometer (CAPS): A new instrument for cloud investigations, Atmos. Res., 59-60, 251-264, 2001.

Baumgardner, D., S. Abel, D. Axisa, R. Cotton, J. Crosier, P. Field, C. Gurganus, A. Heymsfield, A. Korolev, M. Krämer, P. Lawson, G. McFarquhar, J. Z Ulanowski, J. Shik Um,: Chapter 9: Cloud Ice Properties - In Situ Measurement Challenges, AMS Monograph on Ice Formation and Evolution in Clouds and Precipitation: Measurement and Modeling Challenges, Eds. D. Baumgardner, G. McFarquhar, A. Heymsfield, Boston, MA., 2016.

590 Bowen, E. G.: A new method of stimulating convective clouds to produce rain and hail, Quarterly
591 Journal of Royal Meteorological Society, 78, 37–45,1952.

592 Bruintjes, R. T.: A review of cloud seeding experiments to enhance precipitation and some new
593 prospects, Bulletin of the American Meteorological Society, 80, 805-820, 1999.

594 Bruintjes, R. T., Clark, T. L., and Hall, W. D.: The dispersion of tracer plumes in mountainous
595 regions in central Arizona: Comparisons between observations and modeling results, Jounral of
596 Applied Meteorology, 34, 971-988, 1995.

597 Bruintjes, R. T., Salazar, V., Semeniuk, T. A., Buseck, P., Breed, D. W., and Gunkelman, J.:
598 Evaluation of Hygroscopic Cloud Seeding Flares, The Journal of Weather Modification, 44(1), 69–
599 94. https://doi.org/10.54782/jwm.v44i1.85, 2012.

600 Canagaratna, M. R., Jayne, J.T., Jimenez, J.L., Allan, J.D., Alfarra, M.R., Zhang, Q.,
601 Onasch, T.B., Drewnick, F., Coe, H., Middlebrook, A., Delia, A., Williams, L.R., Trimborn, A.M.,
602 Northway, M.J., DeCarlo, P.F., Kolb, C.E., Davidovits, P. and Worsnop, D.R.: Chemical and
603 microphysical characterization of ambient aerosols with the aerodyne aerosol mass spectrometer.
604 Mass Spectrometer Reviews, 26, 185–222, 2007.

605 Cooper, W. A., Bruintjes, R. T. and Mather, G. K.: Calculations pertaining to hygroscopic seeding
606 with flares, Journal of Applied Meteorology, 36, 1449-1469, 1997.

607 DeCarlo, P. F., Kimmel, J. R., Trimborn, A., Northway, M. J., Jayne, J. T., Aiken, A. C., Gonin,
608 M., Fuhrer, K., Horvath, T., Docherty, K.S., Worsnop, D. R. and Jimenez, J. L.: Field-deployable,
609 high-resolution, time-of-flight aerosol mass spectrometer. Analytical Chemistry, 78, 8281–8289,
610 2006.

611 Drewnick, F., Diesch, J. M., Faber, P., and Borrmann, S.: Aerosol mass spectrometry: particle–
612 vaporizer interactions and their consequences for the measurements, *Atmospheric Measurement and*
613 *Techn.,*. 8, 3811-3830, 2015.

614 Flossmann, A., Michael, M., Abshaev, A., Bruintjes R., Masataka, M., Prabhakaran T. and Zhanyu,
615 Y.: Review of advances in precipitation enhancement research, Bulletin of the American
616 Meteorological Society, 100, 1465–1480, 2019.

617 Freud, E. and Rosenfeld, D.: Linear relation between convective cloud drop number concentration
618 and depth for rain initiation, J. Geophys. Res. Atmosphere, 117, D02207, 2012.

619 French, J. R., Friedrich, K., Tessendorf, S. A., Rauber, R. M., Geerts, B., Rasmussen, R. M., Xue,
620 L., Kunkel, M. L. and Blestrud, D. R.: Precipitation formation from orographic cloud seeding.
621 Proceeding of National Academy of Scienmces, United States of America, 115, 1168–1173, 2018.

Friedrich, K., Ikeda, K., Tessendorf, S. A., French, J. R., Rauber, R. M., Geerts, B., Xue, L., Rasmussen, R. M., Blestrud, D. R., Kunkel, M. L., Dawson, N. and Parkinson, S: Quantifying snowfall from orographic cloud seeding, Proc. Natl. Acad. Sci. U. S. A., 117(10): 5190–5195, 2020, doi: 10.1073/pnas.1917204117.

Gayatri, K., Prabhakaran T., Malap N., Konwar M., Gurnule D., Bankar S. and Murugavel P.: Physical evaluation of hygroscopic cloud seeding in convective clouds using in situ observations and numerical simulations during CAIPEEX, Atmos. Res., 284: 106558, 1-17, 2023, DOI:10.1016/j.atmosres.2022.106558.

Ghate,V. P., Albrecht, B. A., Kollias, P., Jonsson, H. H. and Breed, D. W.: Cloud seeding as a technique for studying aerosol-cloud interactions in marine stratocumulus, Geophysical Research Letters, 34, L14807, 2007.

Giordano, M. R., Kalnajs, L. E., Goetz, J. D., Avery, A. M., Katz, E., May, N. W., Leemon, A., Mattson, C., Pratt, K. A., and DeCarlo, P. F.: The importance of blowing snow to halogen-containing aerosol in coastal Antarctica: influence of source region versus wind speed, Atmos. Chem. Phys., 18, 16689–16711, https://doi.org/10.5194/acp-18-16689-2018, 2018.

Golderger, L. A., Pekour, M. S., and Hubbe, J. M.: Counterflow Virtual Impactor (CVI) Inlet Aboard Aircraft (INLETCVI-AIR) Instrument Handbook, DOE/SC-ARM-TR-254, https://www.arm.gov/publications/tech_reports/handbooks/doe-sc-arm-tr-254.pdf, 2020.

Hindman ,E. E.: Water droplet fogs formed from pyrotechnically generated condensation nuclei, J. of Weather. Modif., 10, 77-96, 1978.

Jayne, J. T., Leard, D. C., Zhang, X., Davidovits, P., Smith, K. A., Kolb C. E., and Worsnop, D. R.: Development of an Aerosol Mass Spectrometer for Size and Composition Analysis of Submicron Particles, Aerosol Science and Technology, 33:1-2, 49-70, DOI: 10.1080/027868200410840, 2000.

Khain, A. P, Prabha, T. V., Benmoshe, N., Pandithurai, G. and Ovchinnikov, M.: The mechanism of first raindrops formation in deep convective clouds, J. Geophys. Res., 118, 9123-9140, 2013.

Konwar, M., Maheskumar, R. S., Kulkarni, J. R., Freud, E., Goswami, B. N. and Rosenfeld, D.: Aerosol control on depth of warm rain in convective clouds, J. Geophys. Res., 117, D13204, 2012. doi:10.1029/2012JD017585.

Konwar, M., Prabhakaran, T., Khain, A. and Pinsky, M.: Cloud microphysical structure analysis based on high-resolution in-situ measurements, J. Atmospheric Sci., 78, 2265-2285, 2021.

Konwar, M., Malap, N., Hazra, A., Axisa, D., Prabhakaran, T., and Khain, A.: Measurement of Flare Size Distribution and Simulation of Seeding Effect with a Spectral Bin Parcel Model, Pure and Applied Geophysics, 180, 3019–3034, 2023, https://doi.org/10.1007/s00024- 023-03293-z.

Korolev, A. V., Isaac, G. A., Strapp, J. W., Cober, S. G., and Barker, H. W. : In situ measurements of liquid water content profiles in midlatitude stratiform clouds , Q. J. R. Meteorol. Soc. 133: 1693–1699, 2007, DOI: 10.1002/qj.147.

Kuba, N., and Murakami, M.: Effect of hygroscopic seeding on warm rain clouds–numerical study using a hybrid cloud microphysical model, Atmos. Chem. Phys., 2010, *10*, 3335–3351.

Kulkarni, J. R., Maheshkumar, R. S., Morwal, S. B., Padma Kumari B., Konwar M., Deshpande C.G., Joshi R. R., Bhalwankar R.V., Pandithurai G., Safai P.D., Narkhedkar S.G, Dani K. K., Nath A., Nair, S., Sapre, V.V, Puranik P.V., Kandalgaonkar S., Mujumdar V. R., Khaladkar R.M., Vijayakumar R., Thara P. and B. N.Goswami: The cloud aerosol interaction and precipitation enhancement experiment (CAIPEEX): Overview and preliminary results. Current Science, 12, 413-425, 2012.

Lance, Sara, C. A. Brock, Dave Rogers, and J. A. Gordon.: Water droplet calibration of the Cloud Droplet Probe (CDP) and in-flight performance in liquid, ice and mixed-phase clouds during ARCPAC, Atmospheric Measurement Techniques 3, no. 6, 1683-1706, 2010.

Manton, M., Stone, R. C., Pepler, A., Collins, D. R., Bringi, V. N., Thurai, M., Turner, L. and McRae, D.: The Queensland Cloud Seeding Research Program, Bulletin of the American Meteorological Society, https://doi.org/10.1175/BAMS-D-11-00060.1,75–90, 2012.

Martin, G. M., Johnson, D. W. and Spice, A.: The measurement and parameterisation of effective radius of droplets in warm stratocumulus clouds, J. Atmos. Sci., 51, 1823-1842, 1994.

Mather, G. K., Dixon, M. J. and de Jager, J. M.: Assessing the potential for rain augmentation—the Nelspruit randomized convective cloud seeding experiment, Journal of Applied Meteorology, 35, 1465-1482, 1996.

Mather, G. K., Terblanche, D. E., Steffens, F. E. and Fletcher, L.: Results of the South African cloud seeding experiments using hygroscopic flares, Journal of Applied Meteorology, 36, 1433-1447, 1997.

Nenes , A. , Chuang , P. , Flagan , R. C. and Seinfeld , J. H.: A Theoretical Analysis of Cloud Condensation Nucleus (CCN) Instruments . J. Geophys. Res , 106 , 3449 – 3474, 2001.

Noone, K. J., Ogren, J. A., Heintzenberg, J., Charlson, R. J., and Covert D. S.: Design and calibration of a counterflow virtual impactor for sampling of atmospheric fog and cloud droplets, Aerosol Science and Technology 8(3): 235–244, https://doi.org/10.1080/02786828808959186, 1988.

693 Ogren, J. A., Heintzenberg, J., and Charlson, R. J.: In-situ sampling of clouds with a droplet to
694 aerosol converter. Geophys. Res. Lett., 121–124,12, 1985.

695 Ogren, J. A., Heintzenberg, J., and Charlson, R. J.: Virtual impactor. US Patent No. 4, 689,052,
696 1987.

697 Patade, S., Kulkarni, G., Patade, S., Deshmukh, A., Dangat, P., Axisa, D., Prabha, T. V.: Role of
698 liquid phase in the development of ice phase in monsoon clouds: Aircraft observations and
699 numerical simulations. Atmos. Res., 229, 157–174, 2019.
700 https://doi.org/10.1016/j.atmosres.2019.06.022

701 Patade, S., Prabha, T. V., Axisa, D., Gayatri, K., Heymsfield, A,: Particle size distribution properties
702 in mixed-phase monsoon clouds from in situ measurements during CAIPEEX Jour. of Geophys. Res.
703 Atmos., 120, 19, 2015.

704 Pinsky, M., Khain, A. P.: Effects of in-cloud nucleation and turbulence on droplet spectrum
705 formation in cumulus clouds. Quart. J. Roy. Met. Soc., 128, 1-33, 2002.
706
707 Prabha, T. V., Khain, A., Maheshkumar, R. S., Pandithurai, G., Kulkarni, J. R., Konwar, M, and
708 Goswami, B. N.: Microphysics of premonsoon and monsoon clouds as seen from *in situ*
709 measurements during the Cloud Aerosol Interaction and Precipitation Enhancement Experiment
710 (CAIPEEX), J. Atmos. Sci.,68, 1882–1901, 2011.
711

712 Prabhakaran, T., Murugavel, P., Konwar M., Malap, N., Gayatri, K., Dixit, S., Samanta, S.,
713 Chowdhuri., S., Bera, S., Varghese, M., Rao, J., Sandeep, J., Safai, P. D., Sahai, A. K., Axisa, D.,
714 Karipot, A., Baumgardner, D., Werden, B., Fortner, Ed, Hibert, K., Nair, S., Bankar, S., Gurnule, D.,
715 Todekar, K., Jose, J., Jayachandran, V., Soyam, P. S., Gupta, A., Choudhary, H., Aravindhavel, A.,
716 Kantipudi, S. B., Pradeepkumar, P., Krishnan, R., Nandakumar, K., DeCarlo, P. F., Worsnop, D.,
717 Bhat, G. S., Rajeevan, M., and Nanjundiah, R.: CAIPEEX - Indian cloud seeding scientific
718 experiment , Bulletin of American Meteorological Society, 2023, https://doi.org/10.1175/BAMS-D-
719 21-0291.1

720
721 Roberts , G. C. and Nenes , A.: A Continuous-Flow Streamwise Thermal-Gradient CCN Chamber
722 for Atmospheric Measurements, Aeros. Sci. Tech. , 39, 206 – 221, 2005 .

723 Yau, M.K. and Rogers, R.R.: Short Course in Cloud Physics. 3rd Edition, Butterworth-Heinemann,
724 302 p, 1989.

725 Rosenfeld, D., Axisa, D., Woodley, W. and Lahav, R.: A quest for effective hygroscopic cloud
726 seeding, Jounral of Applied Meteorology and Climatology, 49, 1548-1562, 2010.

727 Rosenfeld, D., Woodley, W. L., Axisa, D., Freud, E., Hudson, J. G., and Givati, A.: Aircraft
728 measurements ofthe impacts of pollution aerosols on clouds and precipitation over the Sierra
729 Nevada, J. Geophys. Res.,113, D15203,doi:10.1029/2007JD009544, 2008.

730 Rosenfeld, D., and Gutman, G.: Retrieving microphysical properties near the tops of potential rain
731 clouds by multispectral analysis of AVHRR data, Atmospheric Res., 34, 259–283, 1994.

732 Ryan,B. F. and King, W. D.: A critical review of the Australian experience in cloud seeding,
733 Bulletin of the American Meteorological Society, 78, 239-254, 1997.
734

735 Salcedo, D., Onasch, T. B., Dzepina, K., Canagaratna, M. R., Zhang, Q., Huffman, J. A., DeCarlo, P.
736 F., Jayne, J. T., Mortimer, P., Worsnop, D. R., Kolb, C. E., Johnson, K. S., Zuberi, B., Marr, L. C.,
737 Volkamer, R., Molina, L. T., Molina, M. J., Cardenas, B., Bernabé, R. M., Márquez, C., Gaffney, J.
738 S., Marley, N. A., Laskin, A., Shutthanandan, V., Xie, Y., Brune, W., Lesher, R., Shirley, T., and
739 Jimenez, J. L.: Characterization of ambient aerosols in Mexico City during the MCMA-2003
740 campaign with Aerosol Mass Spectrometry: results from the CENICA Supersite, Atmos. Chem.
741 Phys., 6, 925–946, https://doi.org/10.5194/acp-6-925-2006, 2006.

742 Segal, Y., Khain, A., Pinsky, M. and Rosenfeld, D.: Effects of hygroscopic seeding on raindrop
743 formation as seen from simulations using a 2000-bin spectral cloud parcel model, Atmospheric
744 Research, 71, 3-34, 2004.

745 Segal, Y., and Pinsky, M. and Khain, A.: The role of competition in raindrop formation.
746 Atmospheric Research, 83, 106-118, 2007.

747 Shingler, T., Dey, S., Sorooshian, A., Brechtel, F. J., Wang, Z., Metcalf, A., Coggon, M.,
748 Mülmenstädt, J., Russell, L. M., Jonsson, H. H., and Seinfeld, J. H.: Characterisation and airborne
749 deployment of a new counterflow virtual impactor inlet, Atmos. Meas. Tech., 5, 1259–1269,
750 https://doi.org/10.5194/amt-5-1259-2012, 2012.

751 Silverman, B. A.: A critical assessment of hygroscopic seeding of convective clouds for rainfall
752 enhancement, Bulletin of the American Meteorological Society, 84, 1219-1230, 2003.

753
754 Stith, J. L., Griffith, D. A., Lynn Rose, R., Flueck, J. A., Miller, Jr. J. R., and Smith, P. L.:
755 Aircraft observations of transport and diffusion in cumulus clouds, Jounral of Applied Meteorology
756 and Climatology, 25, 1959-1970, 1986.

757
758 Stith, J. L., Detwiler, A. G., Reinking, R. F. and Smith, P. L.: Investigating transport, mixing, and
759 the formation of ice in cumuli with gaseous tracer techniques, Atmpshreic Research, 25, 195-216,
760 1990.

761 Tessendorf, S. A.; Bruintjes, R. T., Weeks, C., Wilson, J. W., Knight, C. A., Roberts, R. D. , Peter, J.
762 R., Collis, S., Buseck, P. R., Freney, E., Dixon, M., Pocernich, M., Ikeda, K., Axisa, D., Nelson,
763 E., May, P. T., Richter, H., Piketh, S., Burger, R. P., Wilson, L., Siems, S. T., Manton, M., Stone,
764 R. C., Pepler, A., Collins, D. R. , Bringi, V. N. , Thurai, M., Turner, L. and McRae, D.: The
765 Queensland Cloud Seeding Research Program. Bull. Amer. Meteor. Soc., Vol. 89, pp75–90, 2012,
766 https://doi.org/10.1175/BAMS-D-11-00060.1

767 Wang, B. and Laskin, A.: Reactions between water-soluble organic acids and nitrates in
768 atmospheric aerosols: Recycling of nitric acid and formation of organic salts. J. Geophys. Res., 119,
769 3335-3351, 2014.

770 WMO: Report on the WMO international workshop on hygroscopic seeding: Experimental results,
771 physical processes, and research needs, WMP Rep 35, WMO/TD Rep 1006 36, 68pp, 2000.

772 Xue, L., Weeks, C., Chen, S., Tessendorf, S. A., Rasmussen, R. M., Ikeda, K., Kosovic, B.,
773 Behringer, D., French, J. R., Friedrich, K., Zaremba, T. J., Rauber, R. M., Lackner, C. P., Geerts, B.,
774 Blestrud, D., Kunkel, M., Dawson, N. and Parkinson, S.: Comparison between Observed and
775 Simulated AgI Seeding Impacts in a Well-Observed Case from the SNOWIE Field Program
776 Journal of Applied Meteorology and Climatology, page 345–367, 2022. https://doi.org/10.1175/JAMC-
777 D-21-0103.1
778